CHEMISTRY OF MATERIALS

pubs.acs.org/cm

Article

Chemical Vapor Deposition of Transparent, p-Type Cuprous Bromide Thin Films

Christina M. Chang, Luke M. Davis, Eliza K. Spear, and Roy G. Gordon*

Cite This: https://dx.doi.org/10.1021/acs.chemmater.0c04586

Read Online

ACCESS | Metrics & More | Article Recommendations | Supporting Information

ABSTRACT: The semiconductors CuX (X = Cl, Br, or I) are high-mobility p-type transparent conductors, promising for use in thin film optoelectronic devices such as perovskite photovoltaics. These devices require smooth, pinhole free films that are tens of nanometers thick but uniform across tens of centimeters. Chemical vapor deposition (CVD), an established and scalable process, can provide excellent throughput, conformality, and uniformity on such large areas. However, no prior CVD method could produce continuous thin films of any cuprous halide. We have established such a method, preparing CuBr thin films by reaction between HBr gas and vinyltrimethylsilane(hexafluoroacetylacetonato)copper(I). Our method not only provides the desired device-quality films but also opens up the possibility of a general route to CVD of other metal halides.

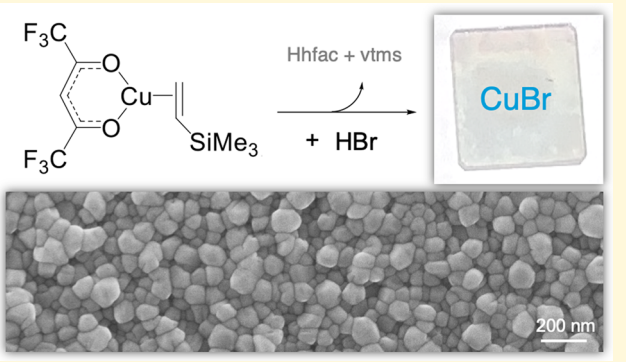

INTRODUCTION

Thin films of transparent conductive layers are important for a wide variety of optoelectronic devices, including photovoltaics and flat-panel displays.[1] These films must be conductive, pinhole free, and optically transparent. Relative to their n-type counterparts, the paucity and low performance of p-type transparent conductors [hole-transport layers (HTLs)] motivate new materials and new methods of thin film preparation.[2,3] Promising emerging materials include SnO,[4] NiO,[5] alloys derived from Cu_2O,[2−5] and the cuprous halides.[6−9]

Chemical vapor deposition (CVD) methods, along with atomic layer deposition (ALD), hold special interest for these applications. CVD is one of the main techniques used in industry to fabricate device-quality films of n-type transparent semiconductors because of its high throughput, conformality, and uniformity on areas up to 3 m wide.[10] However, the CVD methods available for p-type HTLs lag behind those for n-type materials. As an example, in the fast-growing context of perovskite photovoltaics, very few routes exist for CVD or ALD of any HTL.[11] Especially as tandem perovskite-on-Si solar cells move toward commercialization, the implementation of p-i-n configurations[12] will require conformal coatings of transparent HTLs atop textured Si solar cells.[11] Because the HTL can represent half of the cost of a perovskite module,[13] deposition methods compatible with an inexpensive, uniform coverage of large areas could be transformative.

Cuprous halide thin films are increasingly applied as HTLs and provide a synthetic target with a high degree of device relevance. The promising p-type semiconductors CuX (X = Cl, Br, or I) combine near-ultraviolet bandgaps (2.9−3.1 eV),[14] high hole mobility (0.4−12 $cm^2\ V^{-1}\ s^{-1}$ in polycrystalline films),[15,16] and transparency in the visible region. Because of these properties, CuI has been used in p-n junctions,[14] thermoelectric devices,[6] and transparent HTLs in perovskite solar cells;[7] CuBr has been used in thin film transistors[8] and organic photovoltaics.[17] Many solution or physical vapor deposition methods afford CuX thin films,[3] including doctor-blading,[7] spin-coating,[18] vacuum and thermal evaporation,[14,19,20] molecular-beam epitaxy,[21,22] r.f. sputtering,[23,24] and solid or vapor iodination[16,25] of Cu metal or Cu_3N. However, these methods typically produce films that have inadequate smoothness, purity, continuity, or large-area uniformity for commercial application in optoelectronic devices.

The only known CVD or ALD routes to cuprous halides provide either islands or impure films. CVD of CuI from reaction between cyclopentadienyl(triethylphosphino)copper(I) and ethyl iodide results in islands of crystalline CuI.[25] Similarly, ALD or pulsed CVD using surface reactions of [bis(trimethylsilyl)-acetylene](hexafluoroacetylacetonato)copper(I) and HCl or pyridine hydrochloride results in islands of CuCl crystallites.[26−28] We have attempted ALD of CuBr using HBr and the

Received: November 29, 2020
Revised: January 30, 2021

volatile compound bis(*N*,*N*′-di-*sec*-butylacetamidinato)-dicopper(I), $[Cu(sBu_2AMD)]_2$, and found that no film deposits under a variety of conditions.[29] Under pulsed CVD conditions, in which both precursor vapors are available in the reactor simultaneously, the product thin films of CuBr contain substantial carbon and nitrogen owing to acetamidinium bromide formed in an acid−base reaction between HBr and the free acetamidine released during deposition.[29] To the best of our knowledge, continuous thin films of cuprous halides have not yet been attained by CVD.

In fact, just a handful of CVD and ALD processes can produce any metal halide thin films. Several metal fluorides can be deposited by ALD,[30−34] and the first ALD of a metal iodide, PbI_2, was recently reported.[35] CVD can afford films of EuF_3,[36] alloys of titanium and magnesium chlorides,[37] and the lead halide perovskites.[38] We know of no other halide film CVD processes. Accordingly, it is of considerable fundamental and applied interest to develop a more general route to metal halide CVD.

In response to this challenge, we report herein the first CVD of a continuous cuprous halide thin film. Our method uses a reaction between the two commercially available reagents vinyltrimethylsilane(hexafluoroacetylacetonato)copper(I) [Cu(hfac)(vtms)] and HBr. Given the broad availability of volatile metal β-diketonates, this method paves the way for other CVD reactions to produce pure, continuous films of metal halides.

RESULTS AND DISCUSSION

Precursor Selection. We designed the CuBr deposition such that protonation by HBr of a copper(I) complex bearing an anionic ligand releases the neutral form of the ligand and generates CuBr. To avoid contaminating our films with the HBr adduct of the newly released ligand,[29,39] we sought a precursor with a less basic anionic ligand than $[Cu(sBu_2AMD)]_2$. The several copper(I) compounds Cu(hfac)(L),[40] in which L is a neutral Lewis basic ligand, seemed attractive: the pK_a of hexafluoroacetone is 4.6 (in H_2O),[41] much more acidic than unsubstituted acetamidine (pK_a = 27.1 in DMSO).[42] We selected Cu(hfac)(vtms) from among the several Cu(hfac)(L) compounds because vinyltrimethylsilane is less likely to be attacked by HBr (than, say, L = PMe_3), and Cu(hfac)(vtms) is a volatile liquid. Liquid precursors provide better reproducibility of vaporization than solids and are therefore preferred when available.

Screen of Substrates for Deposition. CuBr films were grown in a custom-built, hot-walled ALD reactor (Figures S1 and S2), which has been reported previously.[29] In this reactor, we installed a bubbler containing the Cu(hfac)(vtms) precursor. Thin films of CuBr were deposited via pulsed CVD using alternating exposures of Cu(hfac)(vtms) and HBr, according to the recipes described in the Experimental Section.

The morphology of thin films grown by CVD often depends on the substrate. Cuprous halides do not easily wet metal oxides: we have observed that vapor-converted CuBr forms islands on SiO_2[29] and that CuI forms islands on Cu_2O under many experimental conditions.[39] Similar island growth results have been observed with CVD of CuI on Al_2O_3, SiO_2, Si, and GaAs.[25] We therefore set out to assess our proposed CuX CVD process on alternative, non-oxide substrates that we believed could promote the formation of densely packed, continuous films instead of sparse islands. We were interested in a set of substrates that had low atomic numbers, for Rutherford backscattering spectrometry (RBS); that were optically transparent and electrically insulating, for ultraviolet−visible (UV−vis) spectroscopy and Hall effect measurements, and for ultimate applicability to thin film transistors; and that were metallic, for ultimate applicability to devices like photovoltaics. On the basis of these requirements, availability to our laboratory, and surface free energy considerations that guided our previous vapor conversions to CuX,[39] we selected three substrates for initial tests: glassy carbon, silicon nitride, and platinum. We also deposited upon silica for comparison.

When we ran our standard p-CVD recipe at a substrate temperature of 83 °C, we observed grains approximately 100 nm in diameter on each of the four substrate surfaces (Figure 1). These depositions were uniform across the 1 in. × 1 in.

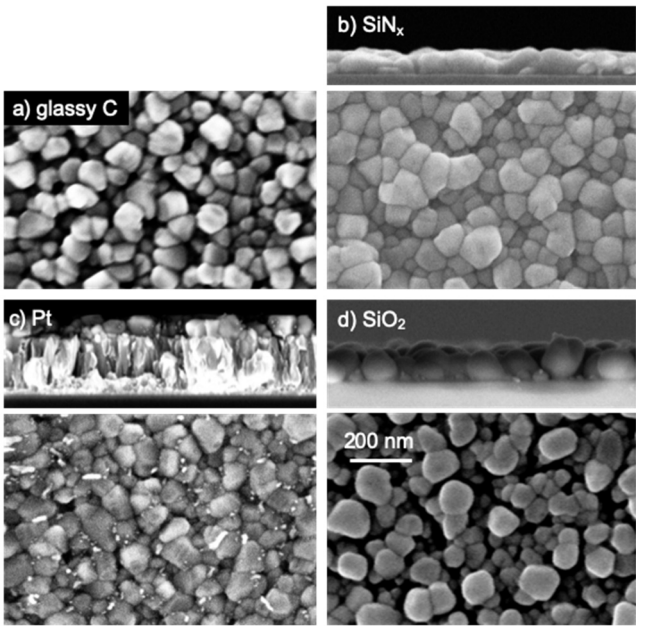

Figure 1. SEM images of CuBr grown at 83 °C on (a) glassy carbon, (b) silicon nitride, (c) platinum, and (d) silica. All films were deposited using 600 cycles of the standard p-CVD recipe. Several fractures of CuBr on carbon planchets did not yield acceptable cross sections. The bright spots in panel c are evidence of a beam-induced phenomenon, described in more detail in the Supporting Information.

substrates (Figures S5 and S6). Consistent with our previous results from vapor-converted CuBr films,[29] we found that CuBr grains on SiO_2 were somewhat isolated from each other, with the SiO_2 substrate visible in the plan-view scanning electron microscopy (SEM) micrographs. In contrast, the ∼70 nm thick CuBr films grown on glassy carbon, silicon nitride, and platinum appeared continuous.

Film Composition Characterization. We next evaluated the elemental composition of the deposited thin films. We first used X-ray photoelectron spectroscopy (XPS). We found that the composition of our film grown on silicon nitride was 55% Cu and 45% Br by XPS (Figure S8). Matrix effects alter the detection efficiency of photoelectrons, and there is no a priori reason to expect the uncalibrated XPS values to be quantitative. Given the difference from the expected 1:1 ratio and the possible role of these matrix effects, we confirmed the composition with RBS. RBS is typically used to detect, in a thin film, elements that are heavier than elements comprising the substrate. Thus, we subjected the film grown on glassy carbon

https://dx.doi.org/10.1021/acs.chemmater.0c04586
Chem. Mater. XXXX, XXX, XXX−XXX

to RBS analysis, allowing us to search for impurities of N, O, etc., to the ~1 atom % level. By RBS, we found that the areal densities of Cu and Br were each $(184 \pm 3) \times 10^{15}$ atoms/cm^2, giving a stoichiometry of $Cu_{1.00}Br_{1.00\pm0.02}$. No other elements heavier than C were detected by RBS. In addition, the peak shapes of the RBS spectra indicated compositional uniformity throughout the CuBr film (Figure S9).

We complemented these composition measurements with X-ray diffraction (XRD). As shown in Figure 2, our CuBr films

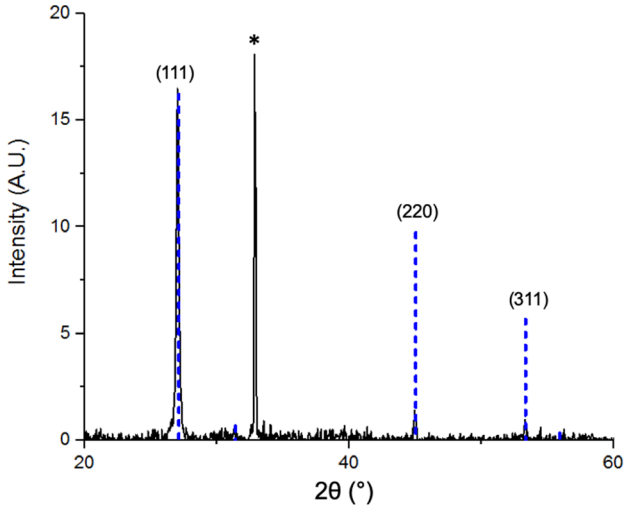

Figure 2. $\theta-2\theta$ XRD diffractogram of CuBr deposited on silicon nitride via 600 cycles of our standard p-CVD recipe. The blue dotted lines from PDF 006-0292, for γ-CuBr, are normalized such that the reference 111 peak height matches our CuBr data 111 peak height. The asterisk denotes a background peak associated with the underlying SiO_2/Si substrate as described in the Supporting Information.

are crystalline and highly oriented in the [111] direction. The experimental pattern matches PDF 006-0292 for γ-CuBr. Using the Scherrer equation, we calculated a value of 43 nm for τ, the mean size of the ordered (crystalline) domains. This value of τ is smaller than the apparent grain size determined by microscopy, which is between 50 and 200 nm for the same film.

Deposition Temperature Study. On the basis of our substrate screen, we chose to further study the deposition characteristics on silicon nitride and platinum substrates. We deposited CuBr using our standard recipe at a range of temperatures between 65 and 200 °C. The size of the CuBr grains increased as a function of temperature, on both silicon nitride (Figure 3 and Figure S10) and platinum (Figure S7).

When CuBr was deposited on silicon nitride, at the high end of the temperature range, e.g. at 136 °C, we observed both a dense layer of 50−100 nm CuBr grains and scattered ~1 μm CuBr particles. These particles are large enough to scatter light, such that the films grown at 110 and 136 °C appear hazy (see Figure 3c,d and Figure S10c,d). In contrast, the films grown at or below 83 °C are transparent. The apparent film haziness increased with substrate temperature: the film grown at 136 °C was hazier than the film grown at 110 °C. The deposition of particles or "powder" is commonly observed in hot-walled CVD reactors.[44,45] Such particles can result when CVD reactions occur between reactants in the gas phase, triggered by high concentrations or high temperatures.[46,47] Light-

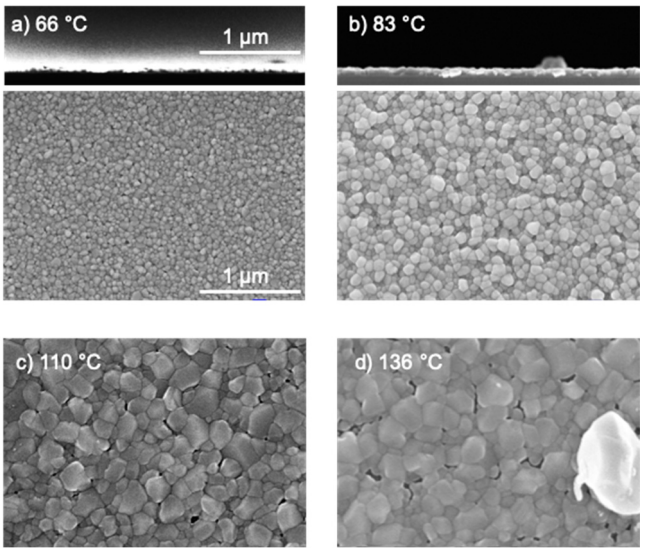

Figure 3. SEM images of CuBr grown on silicon nitride at a range of substrate temperatures: (a) 66, (b) 83, (c) 110, and (d) 136 °C. Scale bars represent 1 μm.

scattering films are not suitable for many applications of transparent conducting layers, so we did not study this reaction at temperatures higher than 136 °C on transparent substrates.

The film morphology also varied with temperature when CuBr was deposited on platinum substrates. As shown in Figure S7, when films were grown by the same standard recipe on platinum substrates, the CuBr grain size and CuBr layer thickness increased with substrate temperature. In particular, the CuBr layer thicknesses were 75 ± 5 nm when grown at substrate temperatures of 66 and 83 °C, but the CuBr grains were significantly larger when grown at the higher substrate temperatures of 163 and 189 °C. At all four substrate temperatures studied, the composition of CuBr films grown on platinum assessed by uncalibrated XPS was approximately 55% Cu and 45% Br (Figure S11). On the basis of our RBS−XPS comparison from CuBr films grown on glassy carbon, these values from XPS suggest that films grown on platinum are also roughly 1:1 Cu:Br.

Though similar CuBr films were deposited on a range of substrates, the mechanism of cuprous bromide film growth might not be the same on all substrates. In particular, although we intended to deposit films by protonolysis of the hfac ligand, the Cu(hfac)(vtms) precursor is known to disproportionate to form Cu and volatile $Cu(hfac)_2$,[48,49] a process promoted by increasing temperature and metal surfaces. This competing reaction pathway for Cu(hfac)(vtms) might occur under our reaction conditions, especially at high temperatures and on the platinum metal substrate. Accordingly, we sought to better understand the CuBr deposition mechanism.

Experiments to Better Understand the Reaction Mechanism. At least two classes of pathways may explain the formation of CuBr via reaction between Cu(hfac)(vtms) and HBr. In the first class, HBr and Cu(hfac)(vtms) undergo an acid−base reaction to form CuBr, Hhfac, and vtms, according to reaction 1:

$$Cu(hfac)(vtms) + HBr \rightarrow CuBr + Hhfac + vtms \quad (1)$$

There are variations on this mechanism depending on when vtms is released and which species are bound to the surface.

https://dx.doi.org/10.1021/acs.chemmater.0c04586
Chem. Mater. XXXX, XXX, XXX−XXX

The second pathway contains two redox reactions. First, two Cu(hfac)(vtms) molecules undergo the known metal-catalyzed disproportionation to form a Cu metal film,[50,51] and the volatile species $Cu(hfac)_2$ and 2 vtms, according to reaction 2:

$$2\ Cu(hfac)(vtms) \rightarrow Cu + Cu(hfac)_2 + 2\ vtms \quad (2)$$

Second, HBr may oxidize the copper metal up to Cu^+, resulting in CuBr and a reduced species, such as H_2, according to reaction 3:

$$2\ Cu + 2\ HBr \rightarrow 2\ CuBr + H_2 \quad (3)$$

We believe the first pathway to be likely by analogy to the many metalorganic precursor reactions with vapors of Brønsted acids (H_2O, H_2S, etc.) to form metal oxides and metal chalcogenides.[52,53] We also explored whether the second pathway might be operational or whether we could rule it out. The second pathway is indeed possible on thermodynamic grounds. Reaction 3 has a ΔG°_{rxn} of −85.5 kJ/mol at 90 °C.[54] However, we reasoned that the Cu metal might not be deposited on a silicon nitride substrate, because the disproportionation of Cu(hfac)(vtms) has been reported only at temperatures above approximately 100 °C and is catalyzed by a metal surface.[48,55,56] This context prompted us to conduct a control experiment to determine whether metallic Cu may be formed on our substrates under our reaction conditions.

In this control experiment, we dosed Cu(hfac)(vtms) into the reactor using the same pulse sequence as the CuBr depositions, but without introducing HBr, at a substrate temperature of 83 °C. The reactor chamber contained five substrates: polished carbon, silica, silicon nitride, alumina, and platinum.

On the four substrates that are not metals (polished carbon, silica, silicon nitride, and alumina), SEM showed essentially no deposition (Figure S18) and XPS identified <1.5 atom % Cu and <0.5 atom % Br on the surfaces of these samples (Figure S19). On the basis of these results, we conclude that the deposition of CuBr on these substrates more likely follows the acid−base mechanism, rather than the two-step deposition of copper followed by bromination.

In contrast, a copper layer had been deposited on the platinum substrate (XPS and SEM micrographs in Figure S20). The thickness of this copper layer varies with distance into the reactor, from ∼300 to ∼80 nm within the first inch of the reactor substrate holder. Therefore, we cannot rule out the two-step deposition mechanism of pathway 2 on Pt substrates. When using the standard recipe, depositions on platinum exhibited more run-to-run variation than depositions on other substrates, perhaps owing to subtleties relating to two available film growth mechanisms.

Growth per Cycle Study. We assessed the CuBr film growth per cycle on silicon nitride substrates at a substrate temperature of 83 °C using two closed-valve p-CVD recipes. Our standard recipe has a 5 s reaction wait time when all valves are closed, whereas in our accelerated recipe, this period is only 0.1 s. These recipes have the same timings for all other pulses, as described in the Experimental Section. When using either recipe, if the Cu(hfac)(vtms) liquid volume in the bubbler was greater than ∼6 mL, we obtained a growth per cycle of 0.12 nm CuBr/cycle for substrates placed at the reactor inlet. However, if the Cu(hfac)(vtms) liquid volume in the bubbler was ≲6 mL, the liquid−gas surface area was smaller, because of the tapered shape of the bubbler bottom. Under this reduced surface area condition, we observed growths per cycle of <0.12 nm/cycle, falling to approximately half of this value at the end of a precursor charge. For both recipes, more CuBr was deposited at the inlet than at the outlet, as described in further detail in the Supporting Information and Figure S16.

From these observations, we conclude that the CVD reaction between Cu(hfac)(vtms) and HBr in our reactor takes place in a precursor-limited growth regime. We reason that the CuBr film thickness decreases along the reactor length from inlet to outlet because one or both precursors are being depleted. Furthermore, the observation of the same film thickness for both 5 and 0.1 s reaction wait times supports the conclusion that the film deposition is not limited by the chemical reaction time under our conditions. One cycle of our accelerated recipe takes 34.55 s, corresponding to a growth rate of 0.2 nm/min.

Seeking to increase this CuBr growth rate, we conducted a brief exploration of a third CuBr deposition recipe, this time employing an open valve between the reaction chamber and vacuum pump. Open-valve recipes can be faster than closed-valve recipes because purging happens simultaneously with precursor dosing. In this recipe, the reactor is constantly purged with nitrogen, and alternating doses of Cu(hfac)(vtms) and HBr are released into the reactor while purging is still occurring. This recipe is described in further detail in the Experimental Section. Our preliminary results suggest that CuBr can be grown using the open-valve mode with a growth per cycle of ≥0.18 nm/cycle. One cycle of this open-valve recipe takes only 10.55 s, corresponding to a growth rate of ∼1 nm/min. Further increases in growth rate may be possible via other modifications to our procedures, such as increasing the precursor partial pressures.

Roughness and Optical Characterization. CuBr thin film samples were prepared in the same deposition for roughness and optical characterization. Two substrates were inserted into the reactor chamber: 40 nm silicon nitride on quartz, which was selected as a transparent substrate for optical characterization, and 40 nm silicon nitride on SiO_2/Si, a witness sample for roughness characterization. The 120 nm thick CuBr films were deposited at a substrate temperature of 83 °C via 1200 cycles of our accelerated recipe.

First, we assessed the roughness of the witness sample by atomic force microscopy (AFM) and found its root-mean-square (RMS) roughness to be 12 nm (see Figures S27 and S28). This value suggested that our films should be relatively nonscattering and smooth enough to be used as transparent conductors for optical applications.[33,43]

Next, we conducted UV−vis spectroscopy on the CuBr grown on the quartz substrate (Figure 4 and Figures S21−S23), confirming that this CuBr sample is mostly transparent in the range of visible light, approximately 400−800 nm. The average transmittance in this region is 79.7% (82.6% below the bandgap ∼2.9 eV). Peaks consistent with the excitonic peaks of CuBr, reported at 2.963 eV (Z_1), 2.972 eV (Z_2), and 3.119 eV (Z_3),[57] are apparent.

Electrical Characterization. Electrical characterization of a CuBr thin film was carried out using an AC Hall effect measurement system. The CuBr sample was 75 nm thick, grown by the accelerated recipe (Figure S13). The sheet resistance for this sample was 5×10^5 Ω/sq, leading us to calculate a resistivity of 3.7 ± 1.0 Ω cm. The charge carrier type was found to be holes. The hole concentration was found to be $(5.5 \pm 1.6) \times 10^{17}$ cm^{-3}, and the hole mobility was

https://dx.doi.org/10.1021/acs.chemmater.0c04586
Chem. Mater. XXXX, XXX, XXX−XXX

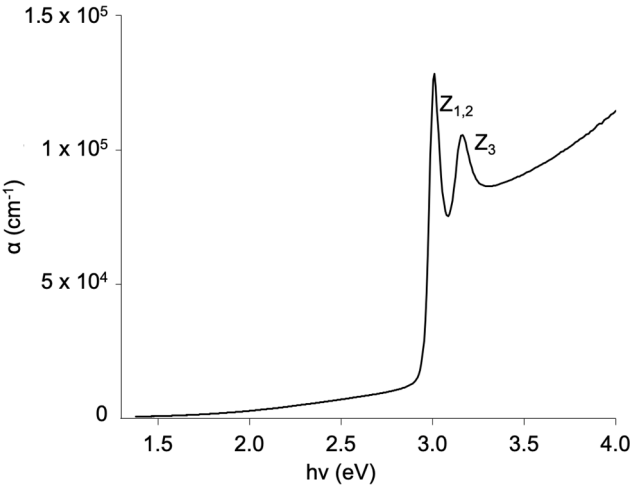

Figure 4. Absorption coefficient vs photon energy for CuBr on 40 nm silicon nitride on quartz, grown using our accelerated recipe at 83 °C. Our CuBr films are mostly transparent in the visible region (1.5−3.0 eV).

measured at 3.0 ± 0.2 cm^2 V^{-1} s^{-1}. Because the carrier concentration is similar to those of previous reports, but the hole mobility is an order of magnitude higher, the resistivity of our sample is an order of magnitude lower than those measured in other polycrystalline Hall samples.[15]

Contact Angle Measurements. Because the substrate strongly affects CuBr film morphology and we and others have attributed such phenomena to film−substrate interfacial free energy matching,[39] we attempted to assess these interfacial free energies based on solid−liquid contact angle measurements.[58,59] The predicted interfacial free energy values between CuBr and the various substrates imply that CuBr should wet Pt and SiO_2 well, silicon nitride and alumina decently, and glassy carbon planchets poorly (Figure S25). In contrast, in our CuBr CVD depositions, CuBr forms continuous films on Pt, silicon nitride, and carbon planchet substrates but forms islands on alumina and silica. These results are further discussed in the Supporting Information.

From the mismatch between the deposited CuBr morphologies and the contact angle measurements, we surmise that these open-air, room-temperature contact angle measurements may not accurately capture the interfacial free energy values of the substrates when under reaction conditions: 83 °C and with reactant headspace gases. In particular, we envision that the chemistry of the reaction is likely to alter the interfacial free energies. For example, the neutral ligand used in Cu(hfac)(vtms), vinyltrimethylsilane, is present in the reactor stoichiometrically with copper(I) and is known to alter the growth versus nucleation rates in the CVD deposition of Cu from Cu(hfac)(vtms).[56] Alternatively, the reaction is run with an excess of HBr, which adsorbs[60] both dissociatively and associatively on Pt below 200 °C—and likely to varying degrees on other materials—which will naturally change the free energy of the substrate surface. Clearly, the surface chemistry under our reaction conditions is more complicated than can be accurately measured outside of the reactor. Our work to understand the in situ surface properties and reactions is ongoing.

CONCLUSION

Using Cu(hfac)(vtms) and HBr as precursors, we report direct chemical vapor deposition of continuous cuprous bromide thin films, which represents the first CuX CVD in the literature to the best of our knowledge. By controlling the growth conditions and choice of substrate, we can produce continuous films of CuBr at low substrate temperatures from 65 to 110 °C, with growth rates of ≤1 nm/min. These films have high optical transparency, exceeding 80% transmittance below their bandgap, and Hall mobilities of approximately 3 cm^2 V^{-1} s^{-1}. The films are therefore suitable for use as transparent p-type semiconductors in optoelectronic devices. A more detailed study of how our reaction chemistry enables continuous film growth is underway. We imagine judicious precursor and substrate choice may similarly enable CVD of a wide range of metal halide thin films.

EXPERIMENTAL SECTION

Purification of Cu(hfac)(vtms). The Cu(hfac)(vtms) compound was received from Gelest as a green liquid mixture of $Cu(hfac)_2$ and Cu(hfac)(vtms). We developed the following procedure to separate the two compounds. In a nitrogen glovebox, the as-received Cu(hfac)(vtms)/$Cu(hfac)_2$ mixture was run through a silica column with pentane as the eluent. We observed a dark green top band and a bright yellow bottom band. The yellow pentane/Cu(hfac)(vtms) solution was collected in a Straus flask, which we sealed and removed from the glovebox. Finally, we submerged the pentane/Cu(hfac)(vtms) solution in an ice bath at 0 °C and removed the pentane by vacuum distillation.[40] We confirmed the remaining mixture was ∼1% pentane via ^{1}H NMR by quantifying all pentane protons and the vinyl protons of Cu(hfac)(vtms). The quantification procedure and ^{1}H NMR spectra are given in the Supporting Information. This ∼99% pure Cu(hfac)(vtms) mixture was used directly as the precursor for CuBr vapor deposition. Purification can be performed on large batches, and the purified precursor stored under nitrogen at −20 °C does not disproportionate appreciably over at least 8 months.

CVD Growth of CuBr. Thin films of CuBr were deposited via pulsed CVD using exposures to Cu(hfac)(vtms) (Gelest, purified as described above) and HBr (Matheson). Cu(hfac)(vtms) was loaded into a vacuum bubbler under a nitrogen atmosphere to prevent decomposition in air. HBr was used as received either at research purity grade (99.999%) or at chemical purity grade (99.8%), in a 1 lb lecture bottle pressurized to 320 psig. Because of the materials used in the construction of the valves, these lecture bottles should not be stored for more than ∼6 months, as the valves tend to corrode due to HBr exposure.

The Cu(hfac)(vtms) vapor was transferred to the reactor chamber by a purified (Entegris purifier model CE500 KFI4R) nitrogen carrier gas held at a pressure of 10 Torr in its trapped volume. Gaseous HBr was delivered using a trapped volume, without a carrier gas. Swagelok ALD valves operated by LABVIEW executed the pulsed CVD recipes. Pulsed CVD is similar to ALD but omits the purging step between precursor doses. We programmed recipes with either of two types of precursor delivery, known in the literature as "open-valve mode" and "closed-valve mode". In open-valve mode, the reactor chamber is constantly being purged with a carrier gas that is being evacuated, such that the valve to the vacuum is never closed. In closed-valve mode, the reactor chamber is closed off from the vacuum at some point in the CVD cycle, typically to "trap" the precursors in the reactor chamber for a longer incubation time than would otherwise be possible if the valve to the vacuum were open. While closed-valve mode may in some instances provide higher precursor utilization and/or greater film coverage and uniformity throughout the reactor, it is also often slower, because it requires separate steps for reaction and for purging/evacuation. We explored both modes.

For closed-valve mode, the timing sequence used for the CuBr recipe may be expressed as t_1−t_2−t_3−t_4−t_5, where t_1 is the dosing time

https://dx.doi.org/10.1021/acs.chemmater.0c04586
Chem. Mater. XXXX, XXX, XXX−XXX

of the Cu(hfac)(vtms), t_2 is the dosing time of the HBr, t_3 is a waiting period during which all valves are closed and deposition occurs, t_4 is the time during which nitrogen purge gas is flushed through the reactor, and t_5 is the chamber evacuation time, with all times given in seconds. For our standard recipe, the timing sequence was 1−1−5−10−20. The purge nitrogen pressure, measured while supplying nitrogen under dynamic vacuum, was 0.7 Torr. Measured in the same way, the pressure of the nitrogen carrier gas was 10 Torr, and the pressure of Cu(hfac)(vtms) alone was 0.04 Torr.

In the standard recipe, the two precursors are in the reactor together for 5 s, resulting in exposure times of 6 s for HBr and 7 s for Cu(hfac)(vtms). To assess the exposure pressures of each precursor, several cycles of the p-CVD recipe were performed. However, instead of opening and closing the valves for both precursors, we opened the valves for only one precursor during each cycle, with all other timing kept the same. The exposure pressure of each gas was adjusted until it was stable at 1 Torr across several cycles. Therefore, the exposures have values of 1 Torr × 6 s = 6 Torr-seconds of HBr and 1 Torr × 7 s = 7 Torr-seconds of Cu(hfac)(vtms)/N_2. The partial pressure of Cu(hfac)(vtms) in this mixture with nitrogen is estimated to be between 0.004 and 0.04 Torr; throughout this range, the HBr is present in excess. The exposure pressures were checked before each deposition but were not adjusted except when new precursor supplies were installed or substantial recipe changes were implemented; typical values fell in the range of 0.1−10 Torr, most commonly ∼2 Torr.

We found during the course of our experiments that the full 5 s of "wait time" is not necessary to achieve our reported growth per cycle. The 5 s wait time t_3 can be reduced to 0.1 s, without reducing the film growth per cycle. Thus, our accelerated closed-valve p-CVD recipe timing sequence is 1−1−0.1−10−20. The exposures of the two precursors therefore decrease from 6 to 1.1 Torr-seconds for HBr and from 7 to 2.1 Torr-seconds for Cu(hfac)(vtms)/N_2.

In open-valve mode, a nitrogen stream is constantly purging the reactor chamber and precursor manifold central lines, so both the house nitrogen valve and the valve to the pump downstream of the reactor chamber are always open. The timing sequence used for an open-valve CuBr recipe may be expressed as t_a−t_b−t_c, where t_a is the dosing time of the Cu(hfac)(vtms)/carrier gas mixture, t_b is the dosing time of the HBr, and t_c is the wait time during which solely the nitrogen and pump valves are open, with all times given in seconds. This wait time is required to return the reactor pressure down to its steady-state nitrogen flow, after HBr and Cu(hfac)(vtms)/carrier gas are dosed in, so that the reactor returns to the same pressure every time the cycle starts. Our open-valve recipe timing sequence is 0.5−0.5−8. The relevant pressures remain the same as for the closed-valve mode. The exposures of HBr and Cu(hfac)(vtms)/N_2 are harder to estimate in this recipe, but the exposure pressures remained set to 1 Torr for each gas.

The control experiments to deposit Cu metal were conducted in closed-valve mode. The timing sequence used for the Cu recipe is the same as our standard closed-valve recipe, namely a timing sequence of 1−1−5−10−20, except that instead of a dose of HBr during the t_2 time, no valves open during that time and thus HBr is not injected into the reactor.

Substrates. Films were deposited on several substrate types. The 12.7 mm diameter highly polished (graphitic) carbon planchets and high-purity vitreous carbon planchets were purchased from Ted Pella. The 1 cm × 1 cm quartz substrates were purchased from Electron Microscopy Sciences. The 1 in. × 1 in. Si substrates with a 300 nm surface layer of SiO_2 grown by wet oxidation were cleaved from larger wafers (University Wafer); all substrates herein described as silica or SiO_2 are of this type. We prepared three more substrate types in house, by adding surface layers to quartz and SiO_2/Si substrates. Platinum surface layers were prepared using a Denton e-beam evaporator: a 5 nm Ti adhesion layer was followed by 200 nm of Pt. Alumina surface layers were 38 nm thick, prepared using a Savannah 200 Thermal ALD reactor. Finally, we prepared silicon nitride surface layers using an STS PECVD:[61] each 40 nm layer of SiN_x was deposited from 35 sccm SiH_4, 55 sccm NH_3, and 1960 sccm N_2 in high-frequency mode (13.56 MHz), with the power supply at 20 W. These silicon nitride substrates undergo partial surface oxidation under our storage conditions as described in the Supporting Information and Figures S14 and S15.

The vitreous (also known as "glassy") and polished carbon planchets were used as received, without washing prior to CuBr deposition. All of the other substrate types were treated with solvent washes of semiconductor-grade acetone and isopropanol (BDH, ≥99%). Furthermore, both the Pt and the SiO_2/Si substrates were then treated with UV−ozone for 5 min both to promote the formation of surface hydroxyl groups and, via oxidation, to further remove any carbonaceous contamination from the surface. Substrates were stored either under ambient conditions but covered (carbon, SiO_2, platinum, and quartz) or in a box purged with nitrogen (silicon nitride).

When prepared for contact angle measurements, substrates were cleaned by ultrasonication in a solvent bath, rather than by a solvent wash. SiO_2 and Pt were sonicated in acetone and isopropanol for 5 min each, followed by 10 min of UV−ozone treatment. SiN_x was sonicated similarly but not subjected to UV−ozone treatment.

Film Characterization. SEM was performed in a Zeiss Ultra Plus scanning electron microscope. XPS was performed on a Thermo Scientific K-Alpha spectrometer equipped with a monochromated Al Kα X-ray source, a 12 kV electron beam, and an Ar^+ sputtering gun. Depth profiles were collected by monatomic sputtering at 500 eV for 80 s per level, unless otherwise indicated. The XPS sputtering rate was determined by dividing the film thickness as determined by SEM cross-sectional film imaging by the total sputtering time before the substrate elemental signals were detected. RBS experiments and data interpretation were conducted at the Rutgers Ion Scattering Facility. A 2.0 MeV beam of $^4He^{2+}$ ions was used for RBS experiments, with an energy resolution of 20 keV. XRD patterns were recorded in a Bruker D2 PHASER X-ray diffractometer using Cu Kα radiation (λ = 1.542 Å) and a θ−2θ scan. AFM topographic images were gathered on a Veeco NanoMan instrument. A 1 Hz scan rate was used in AC mode to produce images of a CuBr film at image sizes of both 1 μm × 1 μm and 10 μm × 10 μm. A grid of 256 points × 256 points was obtained in both cases. Optical transmittance and reflectance measurements were performed over a wavelength range of 200−800 nm using the small spot kit in the diffuse reflectance accessory of an Agilent Cary 7000 Universal Measurement Spectrophotometer. Reflectance measurements were taken at 6°, and transmission measurements at 180°. To determine the absorption coefficient of CuBr thin films, we measured transmittance and reflectance for both a 40 nm SiN_x film on quartz (the "substrate" measurement) and a 120 nm CuBr film on 40 nm SiN_x on quartz (the "total" measurement). To extract the CuBr film absorption coefficient, we used two data treatment steps. First, we calculated α_{sub} and α_{total} via the equation $\alpha = 1/d_{sub} \times \ln[(1 - R)/T]$, where d_{sub} is the thickness of the quartz substrate (1 mm), following the approximation of Ritter and Weiser.[62] Second, we estimated α_{CuBr} via the equation $\alpha_{film} = d_{sub}/d_{film} \times (\alpha_{total} - \alpha_{sub})$, following Cesaria.[63] Electrical properties were assessed by Hall effect measurements using a high-sensitivity rotating parallel dipole line system developed by IBM.[64] To form electrical contacts for Hall measurements, a 10 nm adhesion layer of Ti followed by 200 nm of Au was deposited through a shadow mask by electron-beam evaporation in a Denton Explorer. The leads of the Hall system were adhered to the Au contacts by pressing the wires between thin disks of In solder. Contact angle measurements were performed via the sessile drop technique using the half-angle method on a Tantec CAM-PLUS MICRO instrument equipped with a micrometer syringe and a fiber-optic light source. Four contact angle test liquids (diiodomethane, thiodiglycol, ethylene glycol, and deionized water) were selected for their distinct and well-defined dispersive and polar components of surface free energy.

■ ASSOCIATED CONTENT

Supporting Information

The Supporting Information is available free of charge at https://pubs.acs.org/doi/10.1021/acs.chemmater.0c04586.

https://dx.doi.org/10.1021/acs.chemmater.0c04586
Chem. Mater. XXXX, XXX, XXX−XXX

Experimental setup and temperature measurement details, Rutherford backscattering spectrum, SEM micrographs of CuBr on several substrates at a range of temperatures, photograph of a CuBr thin film and underlying substrates, XPS depth profile analysis of silicon nitride substrates, SEM micrographs and XPS analysis of copper deposition control experiments, UV−vis data, contact angle measurement data, atomic force microscopy data, and other experimental details (PDF)

AUTHOR INFORMATION

Corresponding Author

Roy G. Gordon − *Department of Chemistry and Chemical Biology, Harvard University, Cambridge, Massachusetts 02138, United States; John A. Paulson School of Engineering and Applied Sciences, Harvard University, Cambridge, Massachusetts 02138, United States;* orcid.org/0000-0001-5980-268X; Email: gordon@chemistry.harvard.edu

Authors

Christina M. Chang − *Department of Chemistry and Chemical Biology, Harvard University, Cambridge, Massachusetts 02138, United States;* orcid.org/0000-0002-8824-2834

Luke M. Davis − *Department of Chemistry and Chemical Biology, Harvard University, Cambridge, Massachusetts 02138, United States; Department of Chemistry, Tufts University, Medford, Massachusetts 02155, United States;* orcid.org/0000-0002-8491-0831

Eliza K. Spear − *Department of Chemistry and Chemical Biology, Harvard University, Cambridge, Massachusetts 02138, United States;* orcid.org/0000-0002-1174-8597

Complete contact information is available at: https://pubs.acs.org/10.1021/acs.chemmater.0c04586

Notes

The authors declare the following competing financial interest(s): Harvard University has filed a patent application based on the process described here.

ACKNOWLEDGMENTS

The authors acknowledge the National Science Foundation (NSF) for support of this work under Award CHE 1764338, the E.P.A.-Marshall Scholarship (C.M.C.), and the Draper Laboratory Fellowship (C.M.C.). Some of the work was performed at Harvard's X-ray laboratory and at Harvard University's Center for Nanoscale Systems (CNS), a member of the National Nanotechnology Coordinated Infrastructure Network, which is supported by the NSF under Award ECCS 1541959. The authors gratefully acknowledge Dr. Ryan Thorpe for collecting and analyzing the RBS data. The authors thank Dr. Lauren A. Hartle, Robert I. Gustafson, Dr. Rachel Heasley, Dr. Arthur McClelland, Dr. Shao-Liang Zheng, and J. Cho for helpful conversations and technical assistance.

ABBREVIATIONS

ALD, atomic layer deposition; CVD, chemical vapor deposition; HTL, hole-transport layer; p-CVD, pulsed chemical vapor deposition; RBS, Rutherford backscattering spectrometry; XPS, X-ray photoelectron spectroscopy; XRD, X-ray diffraction; SEM, scanning electron microscopy; SiN_x, silicon nitride; Cu(hfac)(vtms), vinyltrimethylsilane-(hexafluoroacetylacetonato)copper(I)

REFERENCES

(1) Minami, T. Transparent Conducting Oxide Semiconductors for Transparent Electrodes. *Semicond. Sci. Technol.* **2005**, *20* (4), S35−S44.

(2) Zhang, K. H. L.; Xi, K.; Blamire, M. G.; Egdell, R. G. *P*-Type Transparent Conducting Oxides. *J. Phys.: Condens. Matter* **2016**, *28* (38), 383002.

(3) Fioretti, A. N.; Morales-Masis, M. Bridging the P-Type Transparent Conductive Materials Gap: Synthesis Approaches for Disperse Valence Band Materials. *J. Photonics Energy* **2020**, *10* (04), 1.

(4) Ogo, Y.; Hiramatsu, H.; Nomura, K.; Yanagi, H.; Kamiya, T.; Hirano, M.; Hosono, H. *p*-Channel Thin-Film Transistor Using *p*-Type Oxide Semiconductor, SnO. *Appl. Phys. Lett.* **2008**, *93* (3), 032113.

(5) Wang, K.-C.; Jeng, J.-Y.; Shen, P.-S.; Chang, Y.-C.; Diau, E. W.-G.; Tsai, C.-H.; Chao, T.-Y.; Hsu, H.-C.; Lin, P.-Y.; Chen, P.; Guo, T.-F.; Wen, T.-C. p-Type Mesoscopic Nickel Oxide/Organometallic Perovskite Heterojunction Solar Cells. *Sci. Rep.* **2014**, *4*, 4756.

(6) Yang, C.; Souchay, D.; Kneiß, M.; Bogner, M.; Wei, H. M.; Lorenz, M.; Oeckler, O.; Benstetter, G.; Fu, Y. Q.; Grundmann, M. Transparent Flexible Thermoelectric Material Based on Non-Toxic Earth-Abundant p-Type Copper Iodide Thin Film. *Nat. Commun.* **2017**, *8* (1), 16076.

(7) Christians, J. A.; Fung, R. C. M.; Kamat, P. V. An Inorganic Hole Conductor for Organo-Lead Halide Perovskite Solar Cells. Improved Hole Conductivity with Copper Iodide. *J. Am. Chem. Soc.* **2014**, *136* (2), 758−764.

(8) Zhu, H.; Liu, A.; Noh, Y.-Y. Transparent Inorganic Copper Bromide (CuBr) p-Channel Transistors Synthesized From Solution at Room Temperature. *IEEE Electron Device Lett.* **2019**, *40* (5), 769−772.

(9) Yang, C.; Kneiβ, M.; Lorenz, M.; Grundmann, M. Room-Temperature Synthesized Copper Iodide Thin Film as Degenerate p-Type Transparent Conductor with a Boosted Figure of Merit. *Proc. Natl. Acad. Sci. U. S. A.* **2016**, *113* (46), 12929−12933.

(10) Gordon, R. Chemical Vapor Deposition of Coatings on Glass. *J. Non-Cryst. Solids* **1997**, *218*, 81−91.

(11) Raiford, J. A.; Oyakhire, S. T.; Bent, S. Applications of Atomic Layer Deposition and Chemical Vapor Deposition for Perovskite Solar Cells. *Energy Environ. Sci.* **2020**, *13*, 1997−2023.

(12) Stolterfoht, M.; Wolff, C. M.; Marquez, J. A.; Zhang, S.; Hages, C. J.; Rothhardt, D.; Albrecht, S.; Burn, P. L.; Meredith, P.; Unold, T.; Neher, D. Visualization and Suppression of Interfacial Recombination for High-Efficiency Large-Area Pin Perovskite Solar Cells. *Nat. Energy* **2018**, *3* (10), 847−854.

(13) Qiu, L.; He, S.; Ono, L. K.; Liu, S.; Qi, Y. Scalable Fabrication of Metal Halide Perovskite Solar Cells and Modules. *ACS Energy Lett.* **2019**, *4* (9), 2147−2167.

(14) Grundmann, M.; Schein, F.-L.; Lorenz, M.; Bontgen, T.; Lenzner, J.; von Wenckstern, H. Cuprous Iodide - A p-Type Transparent Semiconductor, History, and Novel Applications. *Phys. Status Solidi A* **2013**, *210*, 1671−1703.

(15) Knauth, P.; Massiani, Y.; Pasquinelli, M. Semiconductor Properties of Polycrystalline CuBr by Hall Effect and Capacitive Measurements. *Phys. Status Solidi A* **1998**, *165* (2), 461−465.

(16) Yamada, N.; Ino, R.; Ninomiya, Y. Truly Transparent p-Type γ-CuI Thin Films with High Hole Mobility. *Chem. Mater.* **2016**, *28* (14), 4971−4981.

(17) Bhargav, R.; Chaudhary, N.; Rathi, S.; Shahjad; Bhardwaj, D.; Gupta, S.; Patra, A. Copper Bromide as an Efficient Solution-Processable Hole Transport Layer for Organic Solar Cells: Effect of Solvents. *ACS Omega* **2019**, *4* (3), 6028−6034.

(18) Chen, W.-Y.; Deng, L.-L.; Dai, S.-M.; Wang, X.; Tian, C.-B.; Zhan, X.-X.; Xie, S.-Y.; Huang, R.-B.; Zheng, L.-S. Low-Cost Solution-Processed Copper Iodide as an Alternative to PEDOT:PSS Hole Transport Layer for Efficient and Stable Inverted Planar Hetero-

junction Perovskite Solar Cells. *J. Mater. Chem. A* **2015**, *3* (38), 19353−19359.
(19) Kim, D.; Nakayama, M.; Kojima, O.; Tanaka, I.; Ichida, H.; Nakanishi, T.; Nishimura, H. Thermal-Strain-Induced Splitting of Heavy- and Light-Hole Exciton Energies in CuI Thin Films Grown by Vacuum Evaporation. *Phys. Rev. B: Condens. Matter Mater. Phys.* **1999**, *60* (19), 13879−13884.
(20) Cowley, A.; Lucas, F. O.; Gudimenko, E.; Alam, M. M.; Danieluk, D.; Bradley, A. L.; McNally, P. J. Electroluminescence of γ-CuBr Thin Films via Vacuum Evaporation Deposition. *J. Phys. D: Appl. Phys.* **2010**, *43* (16), 165101.
(21) Yanase, A.; Segawa, Y. Two Different In-Plane Orientations in the Growths of Cuprous Halides on MgO(001). *Surf. Sci.* **1995**, *329* (3), 219−226.
(22) Inagaki, S.; Nakamura, M.; Aizawa, N.; Peng, L. C.; Yu, X. Z.; Tokura, Y.; Kawasaki, M. Molecular Beam Epitaxy of High-Quality CuI Thin Films on a Low Temperature Grown Buffer Layer. *Appl. Phys. Lett.* **2020**, *116* (19), 192105.
(23) Seguin, J.-L.; Bendahan, M.; Lollmun, G.; Pasquinelli, M.; Knauth, P. Preparation of Thin Films of Copper(I) Bromide by r.f. Sputtering: Morphology and Electrical Properties. *Thin Solid Films* **1998**, *323* (1−2), 31−36.
(24) Tanaka, T.; Kawabata, K.; Hirose, M. Transparent, Conductive CuI Films Prepared by rf-dc Coupled Magnetron Sputtering. *Thin Solid Films* **1996**, *281−282*, 179−181.
(25) Gottschalch, V.; Blaurock, S.; Benndorf, G.; Lenzner, J.; Grundmann, M.; Krautscheid, H. Copper Iodide Synthesized by Iodization of Cu-Films and Deposited Using MOCVD. *J. Cryst. Growth* **2017**, *471*, 21−28.
(26) Natarajan, G.; Maydannik, P. S.; Cameron, D. C.; Akopyan, I.; Novikov, B. V. Atomic Layer Deposition of CuCl Nanoparticles. *Appl. Phys. Lett.* **2010**, *97* (24), 241905.
(27) Maydannik, P. S.; Natarajan, G.; Cameron, D. C. Atomic Layer Deposition of Nanocrystallite Arrays of Copper(I) Chloride for Optoelectronic Structures. *J. Mater. Sci.: Mater. Electron.* **2017**, *28* (16), 11695−11701.
(28) Krumpolec, R.; Homola, T.; Cameron, D.; Humlícek, J.; Caha, O.; Kuldova, K.; Zazpe, R.; Prikryl, J.; Macak, J. Structural and Optical Properties of Luminescent Copper(I) Chloride Thin Films Deposited by Sequentially Pulsed Chemical Vapour Deposition. *Coatings* **2018**, *8* (10), 369.
(29) Heasley, R.; Chang, C. M.; Davis, L. M.; Liu, K.; Gordon, R. G. Vapor Deposition of Copper(I) Bromide Films via a Two-Step Conversion Process. *J. Vac. Sci. Technol., A* **2017**, *35* (1), 01B109.
(30) Chen, L.; Chen, K.-S.; Chen, X.; Ramirez, G.; Huang, Z.; Geise, N. R.; Steinruck, H.-G.; Fisher, B. L.; Shahbazian-Yassar, R.; Toney, M. F.; Hersam, M. C.; Elam, J. W. Novel ALD Chemistry Enabled Low-Temperature Synthesis of Lithium Fluoride Coatings for Durable Lithium Anodes. *ACS Appl. Mater. Interfaces* **2018**, *10* (32), 26972−26981.
(31) Lee, Y.; Sun, H.; Young, M. J.; George, S. M. Atomic Layer Deposition of Metal Fluorides Using HF−Pyridine as the Fluorine Precursor. *Chem. Mater.* **2016**, *28* (7), 2022−2032.
(32) Pilvi, T.; Hatanpaa, T.; Puukilainen, E.; Arstila, K.; Bischoff, M.; Kaiser, U.; Kaiser, N.; Leskela, M.; Ritala, M. Study of a Novel ALD Process for Depositing MgF_2 Thin Films. *J. Mater. Chem.* **2007**, *17* (48), 5077−5083.
(33) Mantymaki, M.; Hamalainen, J.; Puukilainen, E.; Sajavaara, T.; Ritala, M.; Leskela, M. Atomic Layer Deposition of LiF Thin Films from Lithd, $Mg(thd)_2$, and TiF_4 Precursors. *Chem. Mater.* **2013**, *25* (9), 1656−1663.
(34) Lee, Y.; DuMont, J. W.; Cavanagh, A. S.; George, S. M. Atomic Layer Deposition of AlF_3 Using Trimethylaluminum and Hydrogen Fluoride. *J. Phys. Chem. C* **2015**, *119* (25), 14185−14194.
(35) Popov, G.; Mattinen, M.; Hatanpaa, T.; Vehkamaki, M.; Kemell, M.; Mizohata, K.; Raisanen, J.; Ritala, M.; Leskela, M. Atomic Layer Deposition of PbI_2 Thin Films. *Chem. Mater.* **2019**, *31* (3), 1101−1109.
(36) Amano, R.; Shiokawa, Y.; Sato, N.; Suzuki, Y. Chemical Vapor Deposition Using Lanthanide β-Diketone Chelates with Difluorodichloromethane. *J. Radioanal. Nucl. Chem.* **1993**, *172* (1), 81−86.
(37) Kim, S. H.; Tewell, C. R.; Somorjai, G. A. Surface Science Studies of Ziegler-Natta Olefin Polymerization System: Correlations between Polymerization Kinetics, Polymer Structures, and Active Site Structures on Model Catalysts. *Korean J. Chem. Eng.* **2002**, *19* (1), 1−10.
(38) Luo, P.; Zhou, S.; Xia, W.; Cheng, J.; Xu, C.; Lu, Y. Chemical Vapor Deposition of Perovskites for Photovoltaic Application. *Adv. Mater. Interfaces* **2017**, *4* (8), 1600970.
(39) Heasley, R.; Davis, L. M.; Chua, D.; Chang, C. M.; Gordon, R. G. Vapor Deposition of Transparent, p-Type Cuprous Iodide Via a Two-Step Conversion Process. *ACS Appl. Energy Mater.* **2018**, *1* (12), 6953−6963.
(40) Chi, K.-M.; Shin, H.-K.; Hampden-Smith, M. J.; Kodas, T. T.; Leo, M. M. D.; Goel, S. C.; Buhro, W. E. Lewis Base Adducts of 1,1,1,5,5,5-Hexafluoro-2,4-Pentandionato-Copper(I) Compounds. In *Inorganic Syntheses*; Cowley, A. H., Ed.; John Wiley & Sons, Inc.: Hoboken, NJ, 2007; pp 289−294.
(41) Linn Belford, R.; Martell, A. E.; Calvin, M. Influence of Fluorine Substitution on the Properties of Metal Chelate Compounds—I Copper(II) Chelates of Bidentate Ligands. *J. Inorg. Nucl. Chem.* **1956**, *2* (1), 11−31.
(42) Bordwell, F. G.; Ji, G. Z. Effects of Structural Changes on Acidities and Homolytic Bond Dissociation Energies of the Hydrogen-Nitrogen Bonds in Amidines, Carboxamides, and Thiocarboxamides. *J. Am. Chem. Soc.* **1991**, *113* (22), 8398−8401.
(43) Ma, Z.; Tang, Z.; Wang, E.; Andersson, M. R.; Inganas, O.; Zhang, F. Influences of Surface Roughness of ZnO Electron Transport Layer on the Photovoltaic Performance of Organic Inverted Solar Cells. *J. Phys. Chem. C* **2012**, *116* (46), 24462−24468.
(44) Collins, J.; Rosner, D. E.; Castillo, J. Onset Conditions for Gas Phase Reaction and Nucleation in the CVD of Transition Metal Oxides. *MRS Proc.* **1991**, *250*, 53.
(45) Simmonds, M. G.; Gladfelter, W. L.; Li, H.; McMurry, P. H. Particle Contamination in Low Pressure Organometallic Chemical Vapor Deposition Reactors: Methods of Particle Detection and Causes of Particle Formation Using a Liquid Alane (AlH_3) Precursor. *J. Vac. Sci. Technol., A* **1993**, *11* (6), 3026−3033.
(46) Tandon, P.; Rosner, D. E. Codeposition on Hot CVD Surfaces: Particle Dynamics and Deposit Roughness Interactions. *AIChE J.* **1996**, *42* (6), 1673−1684.
(47) Artelt, C.; Schmid, H.-J.; Peukert, W. On the Impact of Accessible Surface and Surface Energy on Particle Formation and Growth from the Vapour Phase. *J. Aerosol Sci.* **2005**, *36* (2), 147−172.
(48) Doppelt, P. Copper CVD Precursors and Processes for Advanced Metallization. *Microelectron. Eng.* **1997**, *37−38*, 89−95.
(49) Naik, M. B.; Gill, W. N.; Wentorf, R. H.; Reeves, R. R. CVD of Copper Using Copper (I) and Copper (II) β-Diketonates. *Thin Solid Films* **1995**, *262* (1−2), 60−66.
(50) Doppelt, P.; Baum, T. H. Chemical Vapor Deposition of Copper for IC Metallization: Precursor Chemistry and Molecular Structure. *MRS Bull.* **1994**, *19* (08), 41−48.
(51) Jain, A.; Chi, K.-M.; Kodas, T. T.; Hampden-Smith, M. J. Chemical Vapor Deposition of Copper from Hexafluoroacetylacetonato Copper(I) Vinyltrimethylsilane. *J. Electrochem. Soc.* **1993**, *140* (5), 1434.
(52) Spencer, J. T. Chemical Vapor Deposition of Metal-Containing Thin-Film Materials from Organometallic Compounds. *Prog. Inorg. Chem.* **2007**, 145−237.
(53) Gordon, R. G. ALD Precursors and Reaction Mechanisms. In *Atomic Layer Deposition for Semiconductors*; Springer US: Boston, 2014; pp 15−46. DOI: 10.1007/978-1-4614-8054-9
(54) Haynes, W. M. *CRC Handbook of Chemistry and Physics*, 95th ed.; CRC Press: Boca Raton, FL, 2014.
(55) Burke, A.; Braeckelmann, G.; Manger, D.; Eisenbraun, E.; Kaloyeros, A. E.; McVittie, J. P.; Han, J.; Bang, D.; Loan, J. F.; Sullivan, J. J. Profile Simulation of Conformality of Chemical Vapor

Deposited Copper in Subquarter-Micron Trench and Via Structures. *J. Appl. Phys.* **1997**, *82* (9), 4651−4660.
(56) Babar, S.; Davis, L. M.; Zhang, P.; Mohimi, E.; Girolami, G. S.; Abelson, J. R. Chemical Vapor Deposition of Copper: Use of a Molecular Inhibitor to Afford Uniform Nanoislands or Smooth Films. *ECS J. Solid State Sci. Technol.* **2014**, *3* (5), Q79−Q83.
(57) Madelung, O. Chapter 4: I-VII Compounds. In *Semiconductors: Data Handbook*; Springer: New York, 2004; pp 245−274.
(58) Owens, D. K.; Wendt, R. C. Estimation of the Surface Free Energy of Polymers. *J. Appl. Polym. Sci.* **1969**, *13* (8), 1741−1747.
(59) Girifalco, L. A.; Good, R. J. A Theory for the Estimation of Surface and Interfacial Energies. I. Derivation and Application to Interfacial Tension. *J. Phys. Chem.* **1957**, *61* (7), 904−909.
(60) Garwood, G. A.; Hubbard, A. T. Superlattices Formed by Interaction of Hydrogen Bromide and Hydrogen Chloride with Pt(111) and Pt(100) Studied by LEED, Auger and Thermal Desorption Mass Spectroscopy. *Surf. Sci.* **1981**, *112* (3), 281−305.
(61) Ong, P. L.; Wei, J.; Tay, F. E. H.; Iliescu, C. A New Fabrication Method for Low Stress PECVD - SiN_x Layers. *J. Phys.: Conf. Ser.* **2006**, *34*, 764−769.
(62) Ritter, D.; Weiser, K. Suppression of Interference Fringes in Absorption Measurements on Thin Films. *Opt. Commun.* **1986**, *57* (5), 336−338.
(63) Cesaria, M.; Caricato, A. P.; Martino, M. Realistic Absorption Coefficient of Ultrathin Films. *J. Opt.* **2012**, *14* (10), 105701.
(64) Fai, T. K. Investigating the Open-Circuit Voltage Deficit in $Cu_2ZnSn(S,Se)_4$ Solar Cells. Ph.D. Dissertation, Nanyang Technological University, Singapore, 2015.

https://dx.doi.org/10.1021/acs.chemmater.0c04586
Chem. Mater. XXXX, XXX, XXX−XXX